


## Two-Dimensional Mechanical Metamaterials with Unusual Poisson Ratio Behavior

Zhibin Gao,<sup>1,2</sup> Dan Liu,<sup>1</sup> and David Tománek<sup>1,\*</sup>

<sup>1</sup>Physics and Astronomy Department, Michigan State University, East Lansing, Michigan 48824, USA

<sup>2</sup>Center for Phononics and Thermal Energy Science, China-EU Joint Center for Nanophononics, Shanghai Key Laboratory of Special Artificial Microstructure Materials and Technology, School of Physics, Sciences and Engineering, Tongji University, Shanghai 200092, China

 (Received 16 April 2018; revised manuscript received 4 September 2018; published 17 December 2018)

We design two-dimensional mechanical metamaterials that may be deformed substantially at little or no energy cost. Examples of such deformable structures include assemblies of rigid isosceles triangles hinged at their corners on the macroscale and polymerized phenanthrene molecules forming porous graphene on the nanoscale. In these and in a large class of related structures, the Poisson ratio  $\nu$  diverges for particular strain values. It also changes its magnitude and sign, and displays a shape-memory effect.

DOI: [10.1103/PhysRevApplied.10.064039](https://doi.org/10.1103/PhysRevApplied.10.064039)

### I. INTRODUCTION

There is growing interest in mechanical metamaterials, synthetic structures with counterintuitive mechanical properties [1]. Unlike in ordinary uniform materials, deformations in such metamaterials derive from the geometry of the assembly rather than the elastic properties of the components. This behavior is scale independent, covering structures from the macroscale to the nanoscale. Most attention in this respect seems to be drawn by the Poisson ratio  $\nu$  [2], the negative ratio of lateral to applied strain. Ordinary materials with typical values of  $0 < \nu < 0.5$  contract laterally when stretched, with unusually large values reported for cellular materials [3]. Auxetic metamaterials with  $\nu < 0$ , on the other hand, expand in both directions when stretched [3–7], leading to advanced functionalities [8,9]. Auxetic systems with macroscopic components have been used in automobiles for shock absorption [10], in high-performance clothing [11–13], in bioprotheses [14] and stents [15] in medicine, and for strain amplification [16]. Auxetic two-dimensional (2D) mechanical metamaterials with nanostructured components, some of which were described previously [17–20], may find use when precise micromanipulation of 2D structures including bilayer graphene is required [21].

Here we report the design of 2D mechanical metamaterials that may be deformed substantially at little or no energy cost. Unlike origami- and kirigami-inspired metamaterials, which derive their functionality from the folding of a 2D material into the third dimension [22–25], the structures we describe are confined to a plane during deformation.

Such confinement may be achieved by a strong attraction to a planar substrate or in a sandwich geometry. Specifically, we consider infinite assemblies of rigid isosceles triangles hinged at their corners on the macroscale [26] and polymerized phenanthrene molecules forming “porous graphene” on the nanoscale. In these and in a large class of related structures, consisting of connected and near-rigid isosceles triangles, the Poisson ratio  $\nu$  diverges at particular strain values. It also changes its magnitude and sign, and displays a “shape-memory” effect in a specific range of deformations, meaning that this quantity depends on previously applied strain. Our corresponding results are scale invariant.

### II. COMPUTATIONAL APPROACH

We study the electronic and structural properties as well as the deformation energy of polyphenanthrene, dubbed “porous graphene,” using *ab initio* density functional theory (DFT) as implemented in VASP [27–29]. We represent this 2D structure by imposing periodic boundary conditions in all directions and separating individual layers by a vacuum region of 20 Å. We use projector-augmented-wave pseudopotentials [30,31] and the Perdew-Burke-Ernzerhof (PBE) [32] exchange-correlation functional. The Brillouin zone of the conventional unit cell of the 2D structure is sampled by a  $5 \times 3 \times 1$   $k$ -point grid [33]. We use 500 eV as the electronic kinetic energy cutoff for the plane-wave basis and a total energy difference between subsequent self-consistency iterations below  $10^{-4}$  eV as the criterion for reaching self-consistency. All geometries are optimized by the conjugate-gradient method [34] until none of the residual Hellmann-Feynman forces exceed  $10^{-2}$  eV/Å.

\*tomanek@pa.msu.edu

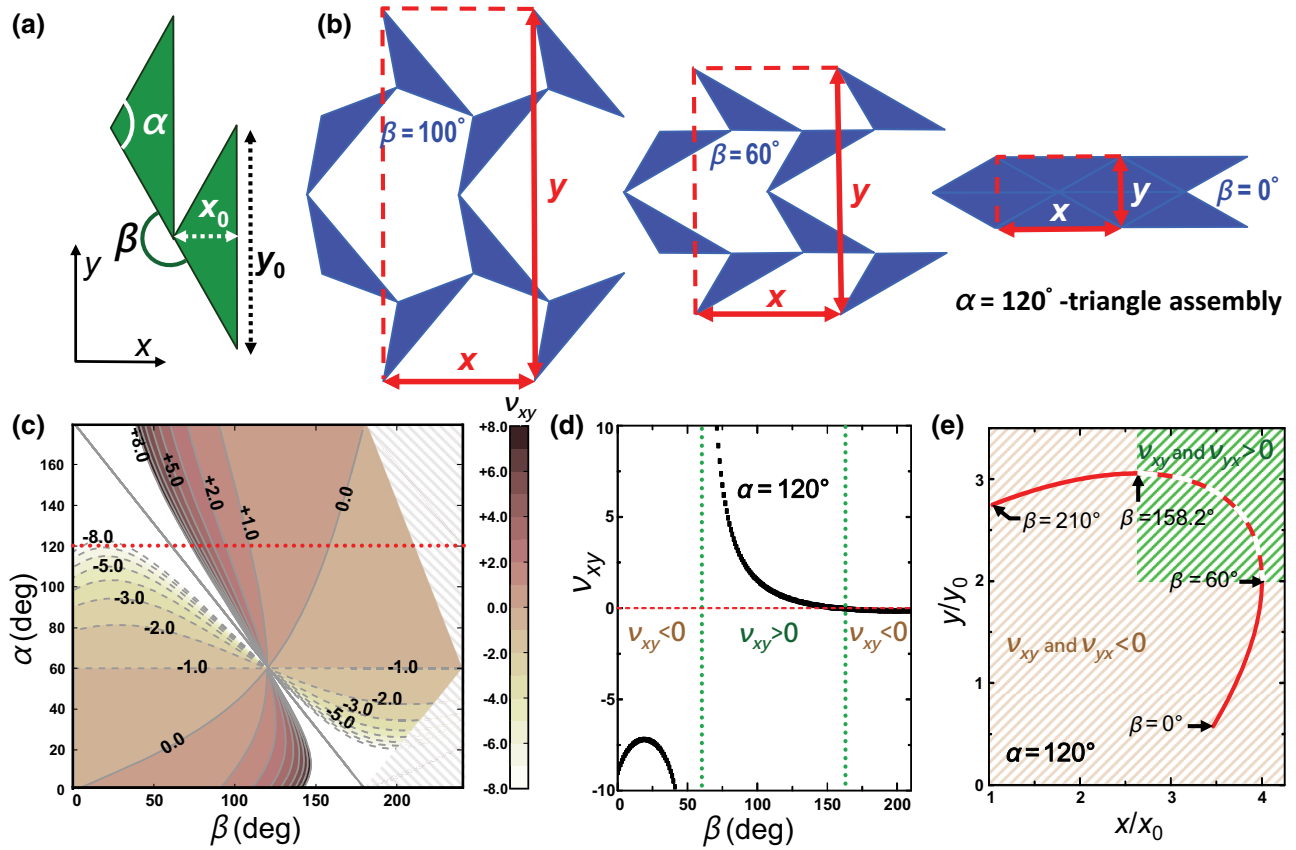


FIG. 1. Deformations in a 2D assembly of rigid isosceles triangles. (a) Adjacent triangles with opening angle  $\alpha$  and mutual orientation defined by the closing angle  $\beta$ , hinged as tip to corner, forming the primitive unit cell. The height  $x_0$  of the triangle and the length  $y_0$  of its base define the horizontal and vertical length scales. (b) Snapshots of the assembly of  $\alpha = 120^\circ$  triangles for different values of  $\beta$ . The conventional rectangular unit cell is twice the size of the primitive unit cell. (c) Contour plot of the Poisson ratio  $\nu_{xy} = -(dy/y)/(dx/x)$  as a function of  $\alpha$  and  $\beta$ . The dotted red line highlights the behavior of the assembly of  $\alpha = 120^\circ$  triangles. (d) Poisson ratio  $\nu_{xy}$  as a function of  $\beta$  in the  $\alpha = 120^\circ$  system. (e) Changes in the scaled width  $x/x_0$  and height  $y/y_0$  of the conventional unit cell for  $\alpha = 120^\circ$  caused by change of the angle  $\beta$ .

### III. RESULTS

#### A. Construction of a 2D mechanical metamaterial

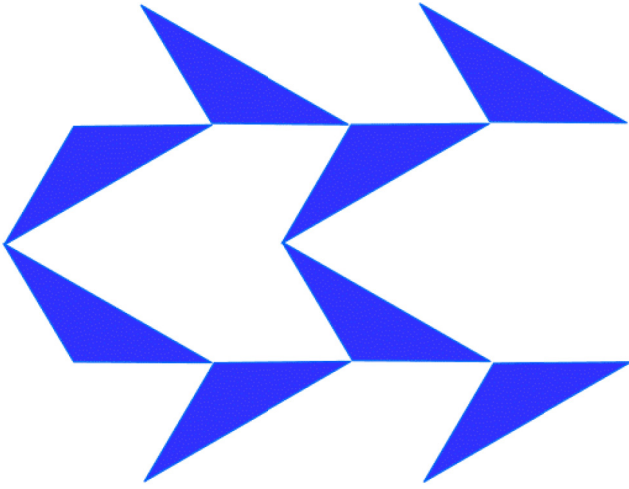
Figure 1 depicts the macroscale 2D mechanical metamaterial we consider, namely, an infinite assembly of rigid isosceles triangles hinged at the corners and described with periodic boundary conditions. There are two identical triangles with different orientation in the primitive unit cell of the lattice, as seen in Fig. 1(a). The conventional unit cell, shown in Fig. 1(b), is rectangular and twice the size of the primitive unit cell. The deformation behavior of such constrained lattices of polygons, including rectangles [35] and connected bars, some of which display a Poisson ratio that changes sign and value and even diverges, was described and classified earlier [26,36]. In our system, structural changes are regulated by the only independent variable, the angle  $\beta$ . The full range of  $\beta$  is  $0 \leq \beta \leq \alpha + 180^\circ$  for  $\alpha \leq 60^\circ$  and  $0 \leq \beta \leq 270^\circ - \alpha/2$  for  $\alpha \geq 60^\circ$ . Since there is no energy involved when  $\beta$  is changed, the structure maintains its geometry after deformation. Snapshots of

the assembly of triangles and the conventional unit cell for different values of  $\beta$ , shown in Fig. 1(b), illustrate the unusual flexibility of the system. A movie of the continuous shape change is provided in Video 1.

For a system of triangles aligned with the Cartesian coordinate system as shown in Fig. 1(a), we can determine the strain in the  $y$  direction in response to strain applied along the  $x$  direction. The negative ratio of these strains is the Poisson ratio  $\nu_{xy}$ , which is given by

$$\begin{aligned} \nu_{xy} &= -\frac{dy/y}{dx/x} \\ &= \frac{\cos(\alpha/2) \sin(\beta/2) - 3 \sin(\alpha/2) \cos(\beta/2)}{\cos(\alpha/2) \cos(\beta/2) + 3 \sin(\alpha/2) \sin(\beta/2)} \tan \\ &\quad \times \left( \frac{\alpha + \beta}{2} \right). \end{aligned} \quad (1)$$

The dependence of  $\nu_{xy}$  on  $\alpha$  and  $\beta$  is presented as a contour plot in Fig. 1(c). Several aspects of this result are



**VIDEO 1.** Unfolding of a 2D assembly of  $\alpha = 120^\circ$  isosceles triangles with changing angle  $\beta$ .

noteworthy when one is inspecting the behavior of  $\nu_{xy}(\beta)$  for a constant value of the opening angle  $\alpha$ . With the exception of  $\alpha = 60^\circ$ , describing equilateral triangles [37,38],  $\nu_{xy}$  changes magnitude and sign with changing  $\beta$ . The presence of the tangent function in Eq. (1) causes  $\nu_{xy}$  to diverge to  $\pm\infty$  for  $\beta_{\text{crit}}(\nu_{xy}) = 180^\circ - \alpha$ , with  $\beta_{\text{crit}}(\nu_{xy}) = 60^\circ$  for  $\alpha = 120^\circ$ . For  $\alpha > 60^\circ$ ,  $\nu_{xy}$  changes sign twice across the full range of  $\beta$  values, as shown in Fig. 1(d) for  $\alpha = 120^\circ$ . The condition for the divergence of  $\nu_{yx} = 1/\nu_{xy}$ , describing strain in the  $x$  direction in response to strain applied in the  $y$  direction, is  $\tan(\beta_{\text{crit}}(\nu_{yx})/2) = 3 \tan(\alpha/2)$ . For  $\alpha = 120^\circ$ ,  $\nu_{yx}$  will diverge at  $\beta_{\text{crit}}(\nu_{yx}) = 158.2^\circ$ .

Maybe the most-unexpected aspect of our result is the shape-memory effect displayed by both  $\nu_{xy}$  and  $\nu_{yx}$  if the angle  $\beta$  becomes a hidden variable in the system. To explain what we mean, we first inspect the  $(x(\beta)/x_0, y(\beta)/y_0)$  trajectory given by

$$\frac{x}{x_0} = 2 \left[ \tan\left(\frac{\alpha}{2}\right) \cos\left(\frac{\beta}{2}\right) + \sin\left(\frac{\beta}{2}\right) \right], \quad (2)$$

$$\frac{y}{y_0} = 3 \sin\left(\frac{\beta}{2}\right) + \cot\left(\frac{\alpha}{2}\right) \cos\left(\frac{\beta}{2}\right). \quad (3)$$

The  $(x(\beta)/x_0, y(\beta)/y_0)$  trajectory, describing the changing shape of the unit cell, is shown for  $\alpha = 120^\circ$  in Fig. 1(e) and for other values of  $\alpha$  in Fig. 4. The sign of the slope of the trajectory, opposite the sign of  $\nu_{xy}$  and  $\nu_{yx}$ , changes twice as the structure unfolds with increasing  $\beta$ . Regions of positive and negative  $\nu_{xy}$  and  $\nu_{yx}$ , delimited by the above-mentioned critical values  $\beta_{\text{crit}}(\nu_{xy})$  for  $\nu_{xy}$  and  $\beta_{\text{crit}}(\nu_{yx})$  for  $\nu_{yx}$ , are distinguished graphically in Fig. 1(e). For any  $x$  in the range  $3.46 < x/x_0 < 4.00$ , there are two different values of  $y$  associated with different values of  $\beta$  and different

signs of  $\nu_{xy}$ . Similarly, for any  $y$  in the range  $2.75 < y/y_0 < 3.06$ , there are two different solutions for  $x$  associated with different values of  $\beta$  and different signs of  $\nu_{yx}$ .

Let us now consider a macroscopic piece of “material” consisting of hinged triangles, which are so small that their mutual orientation cannot be made out. With no information about the deformation history, the material may exhibit either a positive or a negative Poisson ratio. The *only* way to change the material so that it would exhibit a definite positive or negative sign of the Poisson ratio is to subject it to a sequence of deformations. Assume that this material is first stretched to its maximum along a given direction such as  $x$ . Subsequent stretching along a direction normal to the first will result in a positive, subsequent compression with a negative Poisson ratio. We may say that the system retains a memory of previous deformations.

What happens microscopically can be clearly followed in Fig. 1(e). Even though the value of  $\beta$  is hidden, we know that it becomes  $60^\circ$  for maximum stretch along  $x$  and  $158.2^\circ$  for maximum stretch along  $y$ . Subsequent deformation normal to the first direction then dictates the sign of  $\nu$ . This behavior derives from the nonlinearity in the system and, in some aspect, parallels the behavior of shape-memory alloys.

## B. Porous graphene as a 2D mechanical metamaterial

Whereas macroscopic assemblies of triangles with various values of  $\alpha$  will find use in particular applications, we turn our attention to 2D nanostructures that can be formed by coordination chemistry and macromolecular assembly. Microstructures including colloidal kagome lattices [39–41] and graphitic nanostructures [42,43] including polyphenylene [44], sometimes dubbed “nanoporous graphene,” have been synthesized but do not display a negative Poisson ratio. In the following, we focus on polyphenanthrene, a 2D structure of phenanthrene molecules shown in Fig. 2(a). There is a strong similarity between this molecule and the  $\alpha = 120^\circ$  triangles depicted in Fig. 1. In particular, 2D assemblies of the structures in Figs. 1(a) and 2(a) display strong similarities in their Poisson-ratio behavior as discussed below.

The calculated equilibrium structure of 2D porous graphene formed of polymerized phenanthrene molecules with the optimum angle  $\beta = 70^\circ$ , shown in Fig. 2(b), illustrates the relationship between this structure and the assembly of  $\alpha = 120^\circ$  triangles. The unusual flexibility of polyphenanthrene is due to the connection of phenanthrene molecules by strong C—C  $\sigma$  bonds, which are also responsible for the strength and flexibility of polyethylene. Our DFT calculations indicate only small structural distortions of the phenanthrene molecules, which nevertheless break their initial mirror symmetry.

In Fig. 2(c) we compare changes in the scaled width  $x/x_0$  of the conventional unit cell as a function of the closing angle  $\beta$  for the assembly of triangles and for porous

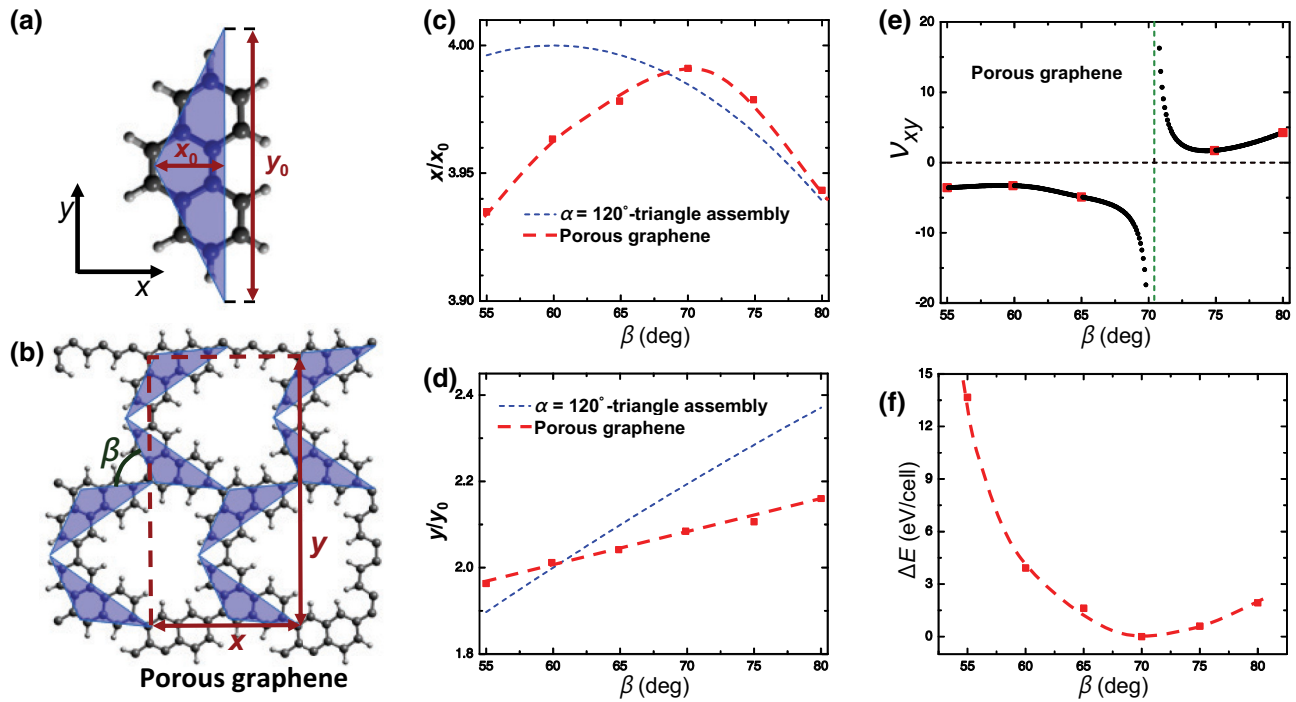


FIG. 2. Deformations in porous graphene, a phenanthrene-based 2D mechanical metamaterial. (a) Structure of the  $C_{14}H_{10}$  phenanthrene molecule and its relation to the  $\alpha = 120^\circ$  isosceles triangle in Fig. 1. (b) Equilibrium structure of 2D porous graphene consisting of polymerized phenanthrene molecules with  $\beta = 70^\circ$ . Saturating hydrogen atoms are shown by the lighter and smaller spheres. Changes in the scaled width  $x/x_0$  (c) and height  $y/y_0$  (d) of the conventional unit cell in the assembly of triangles and porous graphene as a function of the closing angle  $\beta$ . (e) Poisson ratio  $\nu_{xy}$  in porous graphene as a function of  $\beta$ . (f) Strain energy in the  $C_{56}H_{28}$  conventional unit cell as a function of  $\beta$ . The dashed and dotted lines connecting data points for porous graphene in (c)–(f) are guides for the eye.

graphene. The corresponding changes in the scaled height  $y/y_0$  are shown in Fig. 2(d) in the same range of  $\beta$  values. We find  $x(\beta)/x_0$  reaches its maximum at  $\beta_{\text{crit}}(\nu_{xy})$  for both systems, whereas  $y(\beta)/y_0$  increases monotonically with increasing  $\beta$ . According to the definition of the Poisson ratio  $\nu_{xy} = -(dy/y)/(dx/x)$ ,  $\nu_{xy}$  diverges at  $\beta_{\text{crit}}(\nu_{xy}) = 60^\circ$  in the assembly of triangles, as seen in Fig. 1(d). Similarly,  $\nu_{xy}$  diverges at  $\beta_{\text{crit}}(\nu_{xy}) = 70^\circ$  in porous graphene, as shown in Fig. 2(e). The slope of  $x(\beta)/x_0$  changes sign at  $\beta_{\text{crit}}$ , resulting in  $\nu_{xy} < 0$  for  $\beta < \beta_{\text{crit}}(\nu_{xy})$  and  $\nu_{xy} > 0$  for  $\beta > \beta_{\text{crit}}(\nu_{xy})$  in both systems.

The energy investment  $\Delta E$  associated with deforming the polyphenanthrene structure is shown in Fig. 2(f). Our results are obtained by our optimizing the structure for selected values of the angle  $\beta$ , which defines the relative orientation of the two inequivalent phenanthrene molecules in the unit cell. With  $\beta \approx 70^\circ$  representing the structural optimum, we find that changing  $\beta$  by  $\pm 10^\circ$  requires  $\Delta E < 3$  eV per unit cell, corresponding to an energy investment of only approximately 50 meV per C atom, about 1% of the bond-breaking energy. Thus, the polyphenanthrene structure is rather soft and is a valid counterpart to the isoenergetic model system in Fig. 1.

Phenanthrene is a tricyclic organic molecule with a 3.36-eV-wide DFT PBE gap between the lowest unoccupied molecular orbital (LUMO) and the highest occupied molecular orbital (HOMO). When phenanthrene is polymerized to the 2D polyphenanthrene structure depicted in Fig. 2(b), the HOMO broadens to the valence band and the LUMO broadens to the conduction band. This is seen in Fig. 3(a), which depicts the band structure and the density of states of the optimum geometry of polyphenanthrene with  $\beta = 70^\circ$ , with the Brillouin zone shown in the inset. Our DFT PBE results indicate that the fundamental band gap  $E_g$  is reduced from the molecular value to 1.75 eV in the equilibrium structure of the layer, but still does not vanish for  $55^\circ < \beta < 80^\circ$ . The gap is near direct due to the flatness of the bands, and decreases from 1.9 eV at  $\beta = 55^\circ$  to 1.7 eV at  $\beta = 80^\circ$ . We should remember that Kohn-Sham eigenvalues in all DFT calculations, including ours, do not correctly represent the electronic structure and typically underestimate the band gaps.

The decrease of  $E_g$  and its dependence on  $\beta$  on polymerization are caused by the presence of covalent C—C bonds that connect individual phenanthrene molecules elastically and electronically. Unfolding of the polyphenanthrene structure with increasing angle  $\beta$  rotates



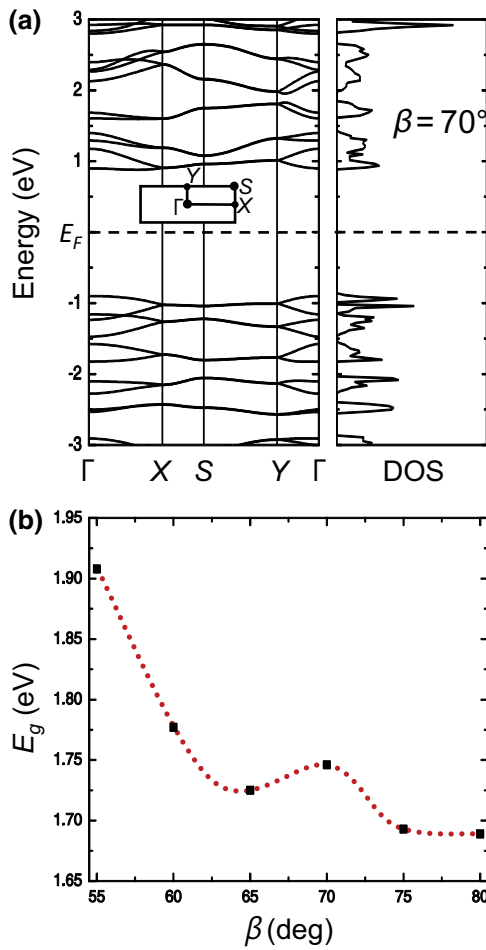


FIG. 3. Electronic structure of porous graphene, a phenanthrene-based 2D mechanical metamaterial, based on DFT PBE calculations. (a) Band structure of the equilibrium structure with  $\beta = 70^\circ$  obtained with the rectangular  $C_{56}H_{28}$  unit cell. High-symmetry points in the rectangular Brillouin zone are shown in the inset. (b) Fundamental band gap  $E_g$  as a function of the angle  $\beta$ . DOS, density of states.

individual phenanthrene molecules and modifies the bonding at the connection between adjacent monomers, causing the electronic structure to depend on  $\beta$ . The range of deformations in polyphenanthrene is smaller than in assemblies of triangles due to the steric hindrance caused by hydrogen termination. In the absence of planar confinement, phenanthrene molecules rotate out of plane at large tensile strain values not considered here.

#### IV. DISCUSSION

Elastic response of materials is commonly described by elastic constants constituting the elastic matrix, which describe stress-strain relationships and thus contain energy in their dimension. The Poisson ratio is fundamentally different. It is a dimensionless quantity that describes deformations induced by strain, independent of the energy cost.

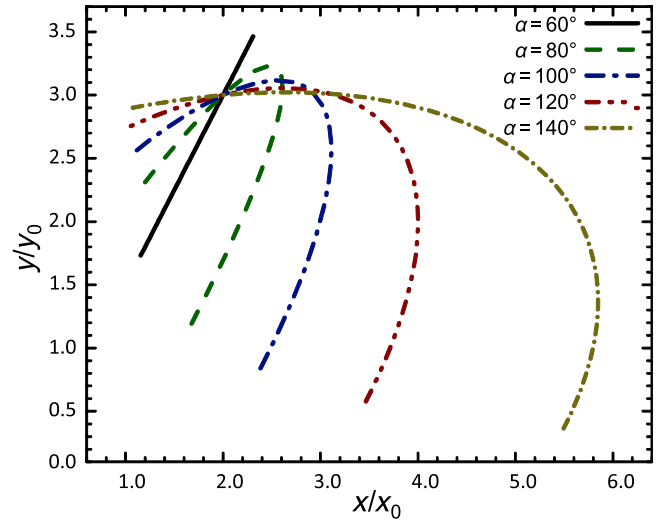


FIG. 4. Changes in the scaled width  $x/x_0$  and height  $y/y_0$  of the conventional unit cell for different values of the opening angle  $\alpha$  as a function of the closing angle  $\beta$ . The relevant quantities are defined in Fig. 1.

According to its definition in Eq. (1), it depends on the choice of the coordinate system. The trace of the strain matrix, however, which describes the fractional change of the area induced by the mechanism, is independent of the choice of coordinates and could couple naturally to external fields such as pressure.

We believe that changes in pore size caused by the deformation of the 2D unit cell may find use in tunable sieving in a layered system [45,46], including application in desalination membranes. Two-dimensional mechanical metamaterials may also find unusual applications in micromanipulation. In particular, a 2D layer in partial contact with an in-plane junction of 2D metamaterials with different values of  $\nu$ , including  $\nu > 0$  and  $\nu < 0$ , may experience a torque normal to the plane when in-plane strain is applied at the junction of the 2D systems. Also, the observation of strain-related electronic structure changes in polyphenanthrene opens new possibilities. Since polyphenanthrene and a wide range of porous-graphene structures can be viewed as a system of covalently connected quantum dots, in-layer strain may be used to tune the coupling between such quantum dots and thus change the electronic structure of the system.

#### V. SUMMARY AND CONCLUSIONS

In summary, we design 2D mechanical metamaterials that may be deformed substantially at little or no energy cost. Unlike origami- and kirigami-based mechanical metamaterials, which derive their functionality from the folding of a 2D material into the third dimension, the

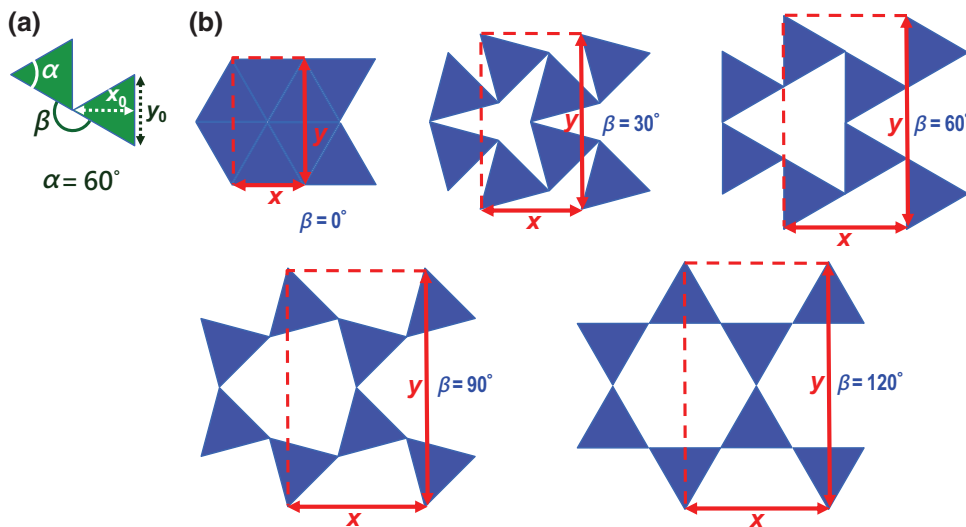


FIG. 5. Deformations in a 2D assembly of rigid equilateral triangles. (a) Adjacent triangles with mutual orientation defined by the closing angle  $\beta$ , hinged at the corners, forming the primitive unit cell. The triangle height  $x_0$  and the length  $y_0$  of its base define the horizontal and vertical length scales. (b) Snap shots of the assembly of triangles for different values of  $\beta$ . The conventional unit cells of width  $x$  and height  $y$  are indicated.

structures we design are confined to a plane during deformation. In reality, such confinement may be achieved by a strong attraction to a planar substrate or in a sandwich geometry. On the macroscale, the structures we describe are assemblies of rigid isosceles triangles hinged at their corners. Their nanoscale counterparts are molecules such as phenanthrene that may be polymerized with use of coordination chemistry or macromolecular assembly to form specific geometries with a porous-graphene structure. In these and in a large class of related structures, consisting of connected and near-rigid isosceles triangles confined to a plane, the Poisson ratio  $\nu$  diverges for particular strain values. It also changes its magnitude and sign, depending on the applied uniaxial strain, and displays a shape-memory effect with respect to the deformation history.

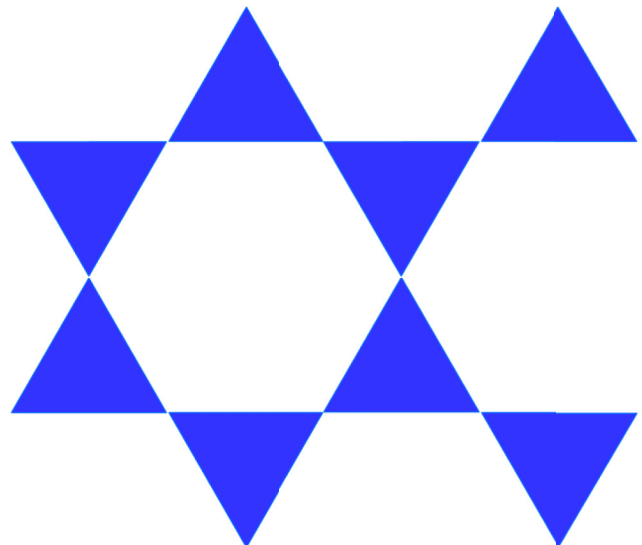
#### APPENDIX A: DEFORMATION BEHAVIOR IN 2D ASSEMBLIES OF ISOSCELES TRIANGLES

As discussed earlier, for a given value  $y$  of the unit cell height in a 2D assembly of isosceles triangles with  $\alpha > 60^\circ$ , we can find two different values of  $x$  of the unit-cell width, with the two structures displaying opposite signs of  $\nu$ . Similarly, we can find two different values of  $y$  for a given value of  $x$ , with the two structures displaying opposite signs of  $\nu$ . This unusual behavior results from the presence of a hidden variable, the relative triangle orientation  $\beta$ , and causes  $\nu$  to depend not only on the overall sample shape but also on the history of the system. The unfolding of an assembly of triangles with  $\alpha = 120^\circ$  and its history dependence are characterized by the  $x$ - $y$  trajectory in Fig. 1(e) in the range of accessible  $\beta$  angles. The unfolding process for the assembly of  $\alpha = 120^\circ$  triangles is depicted in Video 1.

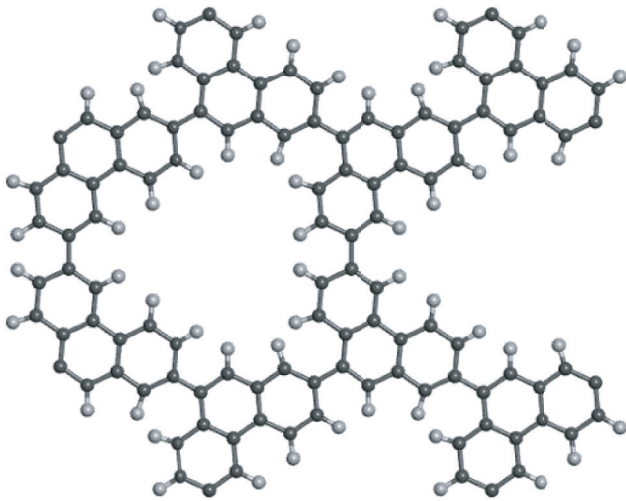
Figure 4 shows  $x$ - $y$  trajectories for several values of  $\alpha$ . The particular shape of these  $x$ - $y$  trajectories indicates that also for opening angles other than  $\alpha = 120^\circ$  discussed above, the value and sign of  $\nu$  may depend on the sample history. Only in the specific case of equilateral triangles with  $\alpha = 60^\circ$ , discussed in the following, is the  $x$ - $y$  trajectory in Fig. 4 linear and is  $\nu$  history independent.

#### APPENDIX B: DEFORMATIONS IN A 2D ASSEMBLY OF RIGID EQUILATERAL TRIANGLES

We mentioned in Appendix A that the behavior of systems of  $\alpha = 60^\circ$  triangles, depicted in Fig. 5, is unique



VIDEO 2. Unfolding of a 2D assembly of  $\alpha = 60^\circ$  equilateral triangles with changing angle  $\beta$ .



**VIDEO 3.** Unfolding of a 2D polyphenanthrene structure dubbed “porous graphene” with changing angle  $\beta$ .

among the 2D assemblies of corner-sharing isosceles triangles. As discussed in the main text and in Appendix A, the Poisson ratio changes drastically for systems of triangles with opening angle  $\alpha$  other than  $60^\circ$ . While hinged equilateral triangles gradually unfold when  $\beta$  increases, as seen in Video 2, the width  $x$  of the unit cell remains proportional to its height  $y$ , resulting in a constant,  $\beta$ -independent Poisson ratio  $\nu_{xy} = -1$ , as noted earlier [37,38]. For the particular angle  $\beta = 120^\circ$ , the structure of the assembly resembles a kagome lattice.

### APPENDIX C: DEFORMATIONS OF 2D POLYPHENANTHRENE

Changes in the 2D polyphenanthrene structure as a function of  $\beta$  are shown in Video 3. The structural changes resemble those shown in Video 1 for the assembly of  $\alpha = 120^\circ$  rigid triangles.

### ACKNOWLEDGMENTS

We thank Jie Ren for useful discussions. D.L. and D.T. acknowledge financial support by the National Science Foundation–Air Force Office of Scientific Research Emerging Frontiers in Research and Innovation Two-Dimensional Atomic-Layer Research and Engineering program (Grant No. EFMA-1433459). Z.G. gratefully acknowledges the China Scholarship Council for financial support (China Scholarship No. 201706260027). Computational resources were provided by the Michigan State University High Performance Computing Center.

- [1] Katia Bertoldi, Vincenzo Vitelli, Johan Christensen, and Martin van Hecke, Flexible mechanical metamaterials, *Nat. Rev. Mater.* **2**, 17066 (2017).
- [2] George Neville Greaves, A. L. Greer, R. S. Lakes, and T. Rouxel, Poisson’s ratio and modern materials, *Nat. Mater.* **10**, 823 (2011).
- [3] Lorna J. Gibson, Michael Farries Ashby, G. S. Schajer, and C. I. Robertson, The mechanics of two-dimensional cellular materials, *Proc. R. Soc. Lond. A* **382**, 25 (1982).
- [4] Roderic Lakes, Foam structures with a negative Poisson’s ratio, *Science* **235**, 1038 (1987).
- [5] Roderic Lakes, Advances in negative Poisson’s ratio materials, *Adv. Mater.* **5**, 293 (1993).
- [6] Ray H. Baughman, and Douglas S. Galvao, Crystalline networks with unusual predicted mechanical and thermal properties, *Nature* **365**, 735 (1993).
- [7] Andrew Alderson, A triumph of lateral thought, *Chem. Ind.* **17**, 384 (1999). <https://pdfs.semanticscholar.org/1e60/eb725884d849ee552de48c8285d55bf91c81.pdf>
- [8] Holger Mitschke, Jan Schwerdtfeger, Fabian Schury, Michael Stingl, Carolin Körner, Robert F. Singer, Vanessa Robins, Klaus Mecke, and Gerd E. Schröder-Turk, Finding auxetic frameworks in periodic tessellations, *Adv. Mater.* **23**, 2669 (2011).
- [9] Zhibin Gao, Xiao Dong, Nianbei Li, and Jie Ren, Novel two-dimensional silicon dioxide with in-plane negative Poisson’s ratio, *Nano Lett.* **17**, 772 (2017).
- [10] Fabrizio Scarpa, Christopher W. Smith, Wayne Miller, Kenneth Evans, and Ramesh Rajasekaran, Vibration damping structures. U.S. Patent US 2012/0315456 A1 (2012).
- [11] Athina Papadopoulou, Jared Laucks, and Skylar Tibbits, Auxetic materials in design and architecture, *Nat. Rev. Mater.* **2**, 17078 (2017).
- [12] Yanyu Chen, Tiantian Li, Fabrizio Scarpa, and Lifeng Wang, Lattice Metamaterials with Mechanically Tunable Poisson’s Ratio for Vibration Control, *Phys. Rev. Appl.* **7**, 024012 (2017).
- [13] Tory M. Cross, Kevin W. Hoffer, David P. Jones, Patrick B. Kirschner, Elizabeth Langvin, and James C. Meschter, Auxetic structures and footwear with soles having auxetic structures. U.S. Patent US 9,402,439 B2 (2016).
- [14] Fabrizio Scarpa, Auxetic materials for bioprostheses [in the spotlight], *IEEE Signal Process. Mag.* **25**, 128 (2008).
- [15] Rudy Hengelmolen, Auxetic tubular liners. U.S. Patent US 2006/0129227 A1 (2006).
- [16] Ray H. Baughman, Justin M. Shacklette, Anvar A. Zakhidov, and Sven Stafström, Negative Poisson’s ratios as a common feature of cubic metals, *Nature* **392**, 362 (1998).
- [17] Sicong Shan, Sung H. Kang, Zhenhao Zhao, Lichen Fang, and Katia Bertoldi, Design of planar isotropic negative Poisson’s ratio structures, *Extreme Mech. Lett.* **4**, 96 (2015).
- [18] David H. Boal, Udo Seifert, and Julian C. Shillcock, Negative Poisson ratio in two-dimensional networks under tension, *Phys. Rev. E* **48**, 4274 (1993).
- [19] K. W. Wojciechowski, Two-dimensional isotropic system with a negative Poisson ratio, *Phys. Lett. A* **137**, 60 (1989).

- [20] Joseph N. Grima, and Kenneth E. Evans, Self expanding molecular networks, *Chem. Commun.* **16**, 1531 (2000).
- [21] Yuan Cao, Valla Fatemi, Shiang Fang, Kenji Watanabe, Takashi Taniguchi, Efthimios Kaxiras, and Pablo Jarillo-Herrero, Unconventional superconductivity in magic-angle graphene superlattices, *Nature* **556**, 43 (2018).
- [22] Mark Schenk, and Simon D. Guest, Geometry of Miura-folded metamaterials, *Proc. Natl. Acad. Sci. U. S. A.* **110**, 3276 (2013).
- [23] H. Yasuda, and J. Yang, Reentrant Origami-Based Metamaterials with Negative Poisson's Ratio and Bistability, *Phys. Rev. Lett.* **114**, 185502 (2015).
- [24] Ahmad Rafsanjani, and Katia Bertoldi, Buckling-Induced Kirigami, *Phys. Rev. Lett.* **118**, 084301 (2017).
- [25] Joseph N. Grima, Szymon Winczewski, Luke Mizzi, Michael C. Grech, Reuben Cauchi, Ruben Gatt, Daphne Attard, Krzysztof W. Wojciechowski, and Jarosław Rybicki, Tailoring graphene to achieve negative Poisson's ratio properties, *Adv. Mater.* **27**, 1455 (2015).
- [26] S. D. Guest, and J. W. Hutchinson, On the determinacy of repetitive structures, *J. Mech. Phys. Solids* **51**, 383 (2003).
- [27] G. Kresse, and J. Furthmüller, Efficient iterative schemes for ab initio total-energy calculations using a plane-wave basis set, *Phys. Rev. B* **54**, 11169 (1996).
- [28] G. Kresse, and J. Furthmüller, Efficiency of ab-initio total energy calculations for metals and semiconductors using a plane-wave basis set, *Comput. Mater. Sci.* **6**, 15 (1996).
- [29] G. Kresse, and J. Hafner, *Ab initio* molecular-dynamics simulation of the liquid-metal–amorphous-semiconductor transition in germanium, *Phys. Rev. B* **49**, 14251 (1994).
- [30] P. E. Blöchl, Projector augmented-wave method, *Phys. Rev. B* **50**, 17953 (1994).
- [31] G. Kresse, and D. Joubert, From ultrasoft pseudopotentials to the projector augmented-wave method, *Phys. Rev. B* **59**, 1758 (1999).
- [32] John P. Perdew, Kieron Burke, and Matthias Ernzerhof, Generalized Gradient Approximation Made Simple, *Phys. Rev. Lett.* **77**, 3865 (1996).
- [33] Hendrik J. Monkhorst, and James D. Pack, Special points for Brillouin-zone integrations, *Phys. Rev. B* **13**, 5188 (1976).
- [34] M. R. Hestenes, and E. Stiefel, Methods of conjugate gradients for solving linear systems, *J. Res. Natl. Bur. Stand.* **49**, 409 (1952).
- [35] J. N. Grima, A. Alderson, and K. E. Evans, Auxetic behaviour from rotating rigid units, *Phys. Status Solidi B* **242**, 561 (2005).
- [36] Graeme Walter Milton, Complete characterization of the macroscopic deformations of periodic unimode metamaterials of rigid bars and pivots, *J. Mech. Phys. Solids* **61**, 1543 (2013).
- [37] Joseph N. Grima, Rosie Jackson, Andrew Alderson, and Kenneth E. Evans, Do zeolites have negative Poisson's ratios? *Adv. Mater.* **12**, 1912 (2000).
- [38] Kai Sun, Anton Souslov, Xiaoming Mao, and T. C. Lubensky, Surface phonons, elastic response, and conformal invariance in twisted kagome lattices, *Proc. Natl. Acad. Sci. U. S. A.* **109**, 12369 (2012).
- [39] Qian Chen, Sung Chul Bae, and Steve Granick, Directed self-assembly of a colloidal kagome lattice, *Nature* **469**, 381 (2011).
- [40] Maeda Hiroaki, Sakamoto Ryota, and Nishihara Hiroshi, Coordination programming of two-dimensional metal complex frameworks, *Langmuir* **32**, 2527 (2016).
- [41] Ryota Sakamoto, Kenji Takada, Tigmansu Pal, Hiroaki Maeda, Tetsuya Kambe, and Hiroshi Nishihara, Coordination nanosheets (conashes): strategies, structures and functions, *Chem. Commun.* **53**, 5781 (2017).
- [42] Matthias Treier, Carlo Antonio Pignedoli, Teodoro Laino, Ralph Rieger, Klaus Müllen, Daniele Passerone, and Roman Fasel, Surface-assisted cyclodehydrogenation provides a synthetic route towards easily processable and chemically tailored nanographenes, *Nat. Chem.* **3**, 61 (2011).
- [43] César Moreno, Manuel Vilas-Varela, Bernhard Kretz, Aran Garcia-Lekue, Marius V. Costache, Markos Paradinas, Mirko Panighel, Gustavo Ceballos, Sergio O. Valenzuela, Diego Peña, and Aitor Mugarza, Bottom-up synthesis of multifunctional nanoporous graphene, *Science* **360**, 199 (2018).
- [44] Marco Bieri, Matthias Treier, Jinming Cai, Kamel Ait-Mansour, Pascal Ruffieux, Oliver Groning, Pierangelo Groning, Marcel Kastler, Ralph Rieger, Xinliang Feng, Klaus Müllen, and Roman Fasel, Porous graphenes: two-dimensional polymer synthesis with atomic precision, *Chem. Commun.* **45**, 6919 (2009).
- [45] Christian Schumacher, Steve Marschner, Markus Cross, and Bernhard Thomaszewski, Mechanical characterization of structured sheet materials, *ACM Trans. Graph.* **37**, 148:1 (2018).
- [46] Daphne Attard, Aaron R. Casha, and Joseph N. Grima, Filtration properties of auxetics with rotating rigid units, *Materials* **11**, 725 (2018).